Infrared Spectroscopy and Elastic Properties of Copper Substituted Nickel Zinc Ferrite

U.M. Mandle[1], L.A. Dhale[2], Ketan A. Ganure[2], B.L. Shinde[3] and K.S. Lohar[2,*]

[1]Department of Chemistry, Sangmeshwar College, Solapur-413 001, India
[2]Department of Chemistry, Shrikrishna Mahavidyalaya, Gunjoti-413 606, India
[3]Department of Chemistry, Waghire College, Saswad-412 301, India

*Corresponding author: E-mail: kslohar@rediffmail.com

Nanocrystalline copper substituted nickel zinc ferrites with composition, $Ni_{0.5}Cu_xZn_{0.5-x}Fe_2O_4$ (x = 0.0, 0.1, 0.2, 0.3, 0.4 and 0.5) synthesized by sol-gel auto combustion technique. All the precursors sintered at 400 °C for 4 h. The stoichiometry and single phase cubic spinel structure confirmed from EDAX and XRD patterns, respectively. Morphology studied by SEM technique. Infrared spectrum of prepared samples investigated at room temperature in the range of 800-300 cm^{-1}. Three major IR absorption bands of tetrahedral frequency in the range of 578-551 cm^{-1}, octahedral frequency in the range of 422-406 cm^{-1} and ν_3 in the range of 352.08 to 325.01 cm^{-1} observed. The stiffness constant (C_{11} and C_{12}), elastic moduli, such as Young's modulus, rigidity modulus, Poisson's ratio and Debye temperature were determined from IR and structural data. The stiffness constant (C_{11} and C_{12}) and elastic moduli decreases while Debye temperature increases with copper substitution.

Keywords: Sol-gel method, Ferrite, Infrared spectroscopy, Elastic property.

INTRODUCTION

Spinel ferrite's structural and magnetic properties are usually modified by altering the compositions of dopants or also by modifying the shape and size of the particles [1]. Copper ferrite has a fundamental application in the nanoscience and technology field such as radio frequency circuits, transformer cores, antennas and read-write heads for high speed digital tape and in high quality filters [2]. Multi-layered chip inductors (MLCI) formation better result obtained due to the copper substituted Ni-Zn ferrites [3]. The nanocrystalline ferrite materials synthesis was day by day increasing due to its desired properties such as geometry, size and stoichiometry better than the bulk material. Structural and magnetic properties depend upon the composition, cation distribution, size and shape of the material [4]. Ni-Zn ferrite is mixed spinel in which tetrahedral (A) sites are occupied by Zn^{2+} and Fe^{3+} ions and octahedral sites (B). This distribution of cations depend on synthesis temperature [5].

Copper shows the coordination geometries such as octahedral, pyramidal, tetrahedral square planar [6]. Cu^{2+} (d^9) ions show the strong John-Teller effect, its substitution in the ferrite

system it preferred to the octahedral (B) sites and it cause the tetrahedral structure distortion [7-9]. In the spinel ferrite lattice, different cations occupied in A and B sites and the force constant determined by using infrared spectroscopy [10,11]. Many researchers have studied the IR spectra for several ferrites. Waldron [12] has also reported the presence of low as well as high-frequency shoulders in his observations. Srinivasan *et al.* [13] investigated the infrared absorption in spinel ferrite. while Zaki and Dawoud [14] studies the far infrared spectra for copper-zinc mixed ferrite used to cation distribution. The elastic properties of its technologically and basic research important for the ferrite. The studies of elastic behaviour to understand the nature of interatomic forces and interionic forces [15]. Herein we report the synthesis of $Ni_{0.5}Cu_xZn_{0.5-x}Fe_2O_4$ (x = 0.0, 0.1, 0.2, 0.3, 0.4, 0.5) by sol-gel auto-combustion method and also examined the effect of Cu^{2+} substituted in Ni-Zn ferrites on the elastic properties.

EXPERIMENTAL

Nanocrystalline copper substituted nickel zinc ferrites, with composition $Ni_{0.5}Cu_xZn_{0.5-x}Fe_2O_4$ synthesized by sol-gel
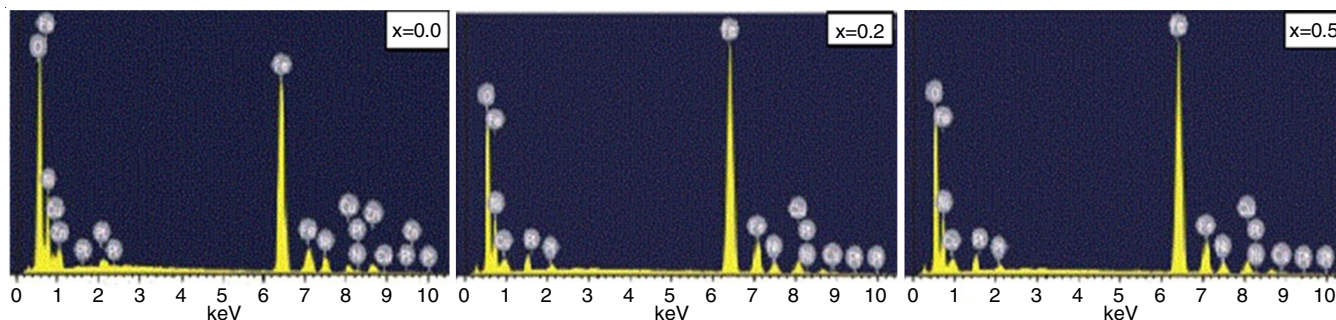
Fig. 1. Energy-dispersive X-ray spectroscopy (EDAX) Patterns, x = 0.0, 0.2 and x = 0.5

auto-combustion method [16]. All the precursors sintered at 400 ºC for 4 h. The elemental stoichiometry was determined by energy dispersive X-ray analysis (EDAX, Inca Oxford). The X-ray powder diffraction patterns were recorded on Philips X-ray diffractometer (Model PW3710) at room temperature by using CuKα radiation. The XRD patterns were recorded at room temperature in 2θ range of 20º-80º with scanning rate 1º/min. The microstructure and morphology of the prepared samples were studied by scanning electron microscopy (SEM) (model JEOL JSM 840). The infrared spectra of all the samples were recorded at room temperature in the range 200 to 800 cm^{-1} using Perkin Elmer infrared spectrophotometer.

RESULTS AND DISCUSSION

Energy dispersive X-ray analysis (EDAX): EDAX patterns of copper substituted nickel zinc nano-spinel ferrites with chemical composition of $Ni_{0.5}Cu_xZn_{0.5-x}Fe_2O_4$ (x = 0.0, 0.3 and 0.5) is shown in Fig. 1. The observed percentage of elements are in close agreement with the composition of theoretical values as listed in Table-1.

SEM analysis: SEM micrographs of sintered copper substituted nickel zinc nano-spinel ferrites (x = 0.2 and 0.5) are shown in Fig. 2, illustrates the fine crystallite structure with weak agglomeration due to high reactivity.

X-ray diffraction: X-ray diffraction (XRD) patterns of $Ni_{0.5}Cu_xZn_{0.5-x}Fe_2O_4$ spinel ferrite system with x = 0.0 to 0.5, in the steps of 0.1 are shown in Fig. 3. The XRD patterns confirmed the formation of single phase cubic spinel structure of ferrites (JCPDS No. 48-0492) [17] without additional peaks consequent to any other phases. The crystal structures of copper substituted nickel zinc ferrite are identified as cubic spinel (space group: fd^{3}m) with the matching (220), (311), (222), (400), (422), (333) and (440) planes.

The results revealed that after the addition of small amount of Cu^{2+} ions, the lattice constant decreases. The values of lattice parameter 'a' listed in Table-2. The calculated value of lattice
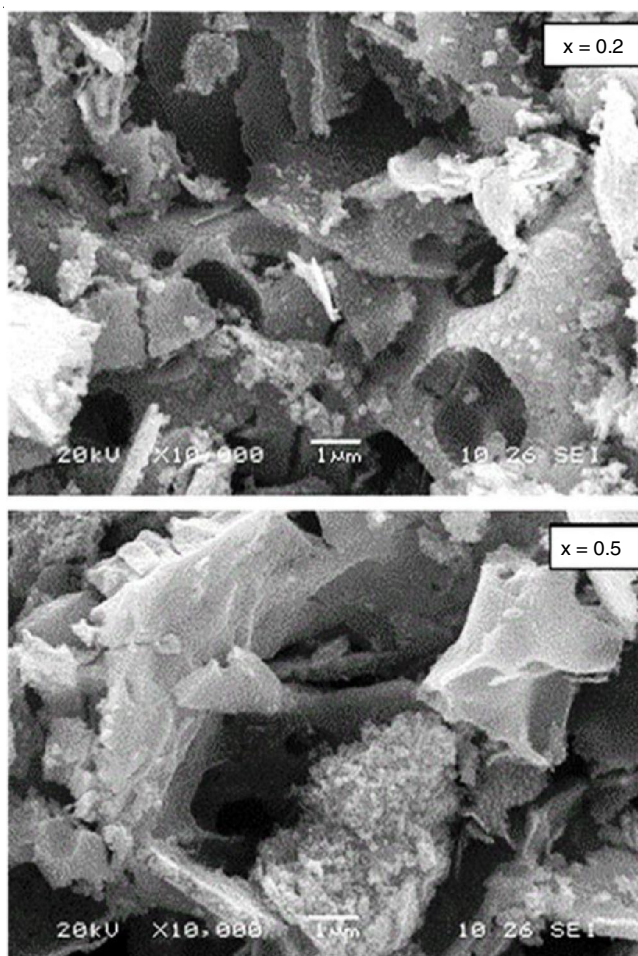
Fig. 2. Scanning electron microscopy (SEM) images, x = 0.2 and 0.5

parameter shows that the samples are to be cubic spinel structure. The lattice constant decreases with Cu^{2+} concentration. The decrease in the lattice constant is related to the difference in ionic radii of Zn^{2+} and Cu^{2+}. In the present ferrite system,

TABLE-1
THEORETICAL AND OBSERVED ELEMENTAL ANALYSIS FROM EDAX OF $Ni_{0.5}Cu_xZn_{0.5-x}Fe_2O_4$

x	Theoretical value (%)					Observed value (%)				
	Ni	Cu	Zn	Fe	O	Ni	Cu	Zn	Fe	O
0.0	12.34	0.00	13.75	46.98	26.93	12.29	0.00	13.98	46.97	26.76
0.1	12.35	2.68	11.01	47.02	26.94	12.44	2.61	11.12	47.02	26.81
0.2	12.36	5.35	8.26	47.06	26.97	12.47	5.27	8.37	47.06	26.83
0.3	12.37	8.04	5.52	47.09	26.98	12.49	8.02	5.45	47.11	26.93
0.4	12.38	10.73	2.76	47.13	27.00	12.51	10.62	2.72	47.08	27.07
0.5	12.39	13.42	0.00	47.17	27.02	12.53	13.11	0.00	47.15	27.21

TABLE-2
LATTICE CONSTANT (a), X-RAY DENSITY (d_x), BAND POSITION (ν_1, ν_2 AND ν_3),
FORCE CONSTANT (K_o AND K_t) OF $Ni_{0.5}Cu_xZn_{0.5-x}Fe_2O_4$

x	'a' (Å)	'd_x' (g/cm³)	Band position					Force constant	
			ν_1 (cm⁻¹)	ν_2 (cm⁻¹)	ν_3 (cm⁻¹)	R_A	R_B	$K_o \times 10^5$ (dyne/cm)	$K_t \times 10^5$ (dyne/cm)
0.0	8.394	5.34	578.231	422.834	335.390	0.3563	0.2959	1.108	1.544
0.1	8.345	5.429	576.231	417.769	325.966	0.3562	0.2958	1.089	1.510
0.2	8.334	5.446	569.702	416.764	358.063	0.3561	0.2958	1.091	1.452
0.3	8.328	5.454	566.503	412.705	361.528	0.3561	0.2957	1.077	1.412
0.4	8.311	5.463	563.038	411.170	346.068	0.3560	0.2957	1.076	1.372
0.5	8.310	5.484	551.043	406.694	352.998	0.3559	0.2957	1.060	1.301

Fig. 3. XRD patterns of $Ni_{0.5}Cu_xZn_{0.5-x}Fe_2O_4$, x = 0.0 to 0.5
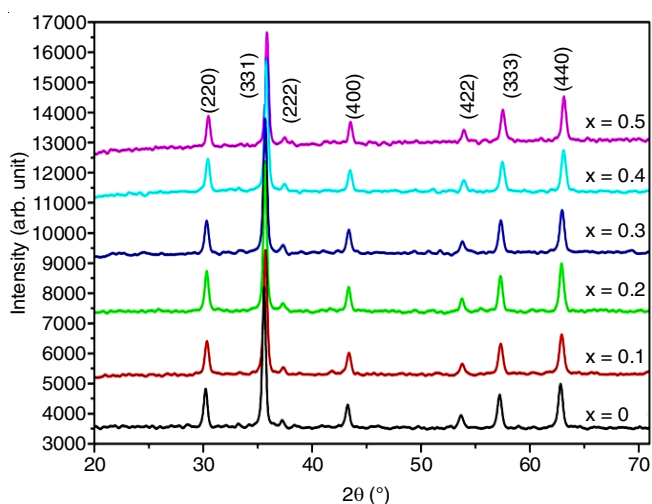
Fig. 4. Infrared spectra of $Ni_{0.5}Cu_xZn_{0.5-x}Fe_2O_4$, x = 0.0 to 0.5

Zn^{2+} ions (0.74 Å) ions are replaced by the relatively smaller Cu^{2+} ions (0.72 Å) [18]. Here Cu^{2+} is substituted for Zn^{2+}. In addition, the existence of Cu and Fe in B-site can result in the John Teller distortion of the octahedral symmetry of B-sites which might lead to a crystal lattice distortion in the ferrites that causes the value of 'a' to decrease [19]. The values of lattice parameter revealed an almost linear dependence, thus obeying Vegard's law [20]. The values of X-ray density are shown in Table-2. The X-ray density also increased with increasing Cu^{2+} content x. The increased in X-ray density is attributed to decrease in lattice constant. It is observed that X-ray density increase for x = 0.5. This may be related to the molecular weight of sample overtakes the volume (a³). The atomic weight of Cu^{2+} ion (63.55 amu) is higher than Zn^{2+} ions (55.84 amu) due to this increases in the X-ray density 5.340 to 5.484g/cm³ [18].

Infrared analysis: The infrared analysis provides the crystal information such as vibration modes and ions occupied in the lattice sites. The ferrite substitution due to metal ions resulted to changes in the unit cell while the whole crystal is not affected. This structural change strongly affected the vibrations modes within the crystal [12]. The IR spectra of copper substituted nickel zinc nano-spinel ferrites are shown in Fig. 4 were recorded at room temperature in the frequency range 800-200 cm⁻¹. The IR spectra illustrated the three major absorption bands as listed in Table-2. The highest ν_1, is observed in the range 600-500 cm⁻¹, and it corresponds to stretching vibrations of the metal at the tetrahedral site M-O, while ν_2 lowest band is usually observed in the range 450-385 cm⁻¹, is assigned to octahedral-metal stretching (M-O) [21].
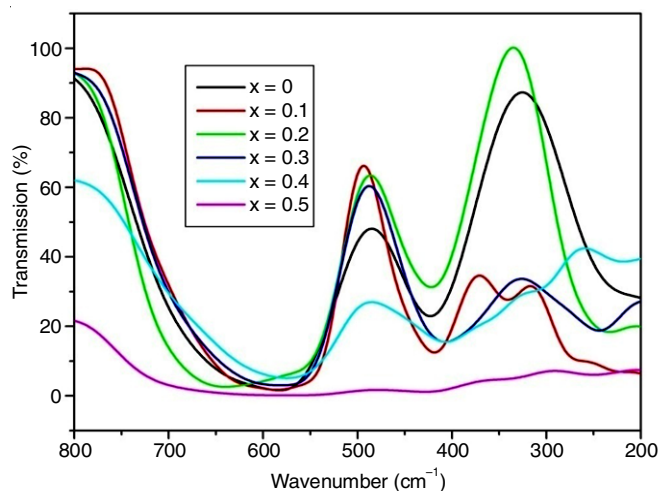
The absorption band frequency ν_1 decreases with an increase in copper concentration (x). This variation in the band positions may be due to the variation in the cation-oxygen bond length [14], which results in a decrease in the frequency of ν_1 band. The octahedral band has a constant value of around 395 cm⁻¹ and this may be due to the neutralization effect for the migration of both Cu^{2+} and Fe^{2+} ions to this site. The octahedral vibration frequency (ν_2) can attributed due to to John-Teller effect in the octahedral site of Cu^{2+} ions, cause to crystal lattice distortion [22]. The ligand lying in z-axis is due to the shortening of band. The lower band ν_3 observed in the range of 352.08 to 325.01 cm⁻¹ is related to divalent Cu^{2+}–O^{2-} bond in the complex [23].

The bond lengths R_A and R_B have been calculated using the formula given by Gorter [12,24] as follows:

$$R_A = \left(u - \frac{1}{4}\right)a_{th}\sqrt{3} - R_o \tag{1}$$

$$R_B = \left(\frac{5}{8} - u\right)a_{th} - R_o \tag{2}$$

The values of bond lengths for tetrahedral A-site (R_A) and octahedral B-site (R_B) were calculated and shown in Table-2. The bond lengths R_A and R_B decrease with increase in the composition of Cu^{2+} ion content. Decrease in the lattice constant by the increasing value of x; this is in coherence with the bigger ionic radii of Zn ions, which has been replaced by a smaller one for the copper ions [14].

The force constants corresponding to tetrahedral and octahedral complexes are calculated by using the standard formulae [12] as given below:

$$K_t = 7.62 \times M_1 \times \nu_1^2 \times 10^{-2} \tag{3}$$

$$K_o = 10.62 \times \frac{M_2}{2} \times \nu_2^2 \times 10^{-2} \tag{4}$$

where K_o is the force constant on octahedral site, K_t is the force constant on tetrahedral site, M_1 is the molecular weight of tetrahedral site, M_2 is the molecular weight of octahedral site, ν_1 is the corresponding centre frequency on tetrahedral site and ν_2 is the corresponding center frequency on octahedral site.

The molecular weights M_1 and M_2 for each sample were determined from the cation distribution. The force constant is the second derivative of the potential energy with respect to the site radius with the other independent parameters kept constant. The force constants values (K_t and K_o) are listed in Table-3. The force constant K_t increases with the increasing Cu^{2+} content whereas K_o decreases with the increasing in Cu^{2+} content. This variation can be related with the difference in ionic radii of Zn^{2+} and Cu^{2+} ions and their occupancy at A and B sites [14]. Analysis of IR spectra with crystallographic knowledge helps us to determine the Debye temperature and elastic properties. The Debye temperature (ν_l) of all samples was determined [25] using the wave numbers of IR bands:

$$\theta l = \frac{\hbar C \nu_{ac}}{\kappa} \tag{5}$$

where $\hbar$ = h/2p, κ is Boltzmann constant, C is velocity of light (C = 3×10^8 cm/s) and ν_{av} is average wave number of bands. Variation of Debye temperature with Cu^{2+} content is shown in Fig. 5.

TABLE-3
MEAN FORCE CONSTANT (K), PORE FRACTION, STIFFNESS CONSTANT (C_{11} AND C_{12}) OF $Ni_{0.5}Cu_xZn_{0.5-x}Fe_2O_4$

x	Mean force constant (K) ($K_t + K_o$)	Pore fraction	Passion's ratio σ	C_{11}	C_{12}
0.0	1.326	0.142	0.276	158.01	60.24
0.1	1.299	0.138	0.277	155.71	59.77
0.2	1.272	0.132	0.279	152.59	59.16
0.3	1.245	0.128	0.281	149.48	58.35
0.4	1.224	0.125	0.282	147.31	57.79
0.5	1.181	0.111	0.286	142.07	57.05
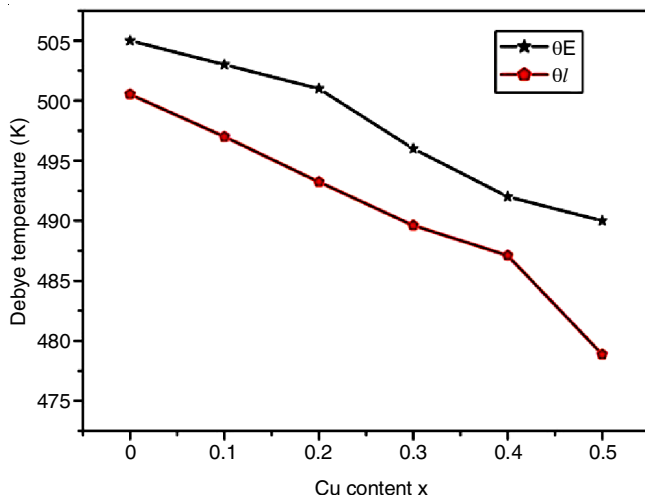
Fig. 5. Variation of Debye temperature determined from infrared (θl) and elastic (θE) data with Cu^{2+} content

Elastic properties: The elastic properties were determined using infrared spectroscopy [26,27]. The elastic modules and Debye temperature were determined by using the IR and structural data [28]. These elastic moduli were determined using the lattice constant 'a', X-ray density 'dx' pore fraction 'f' and force constant 'k'. The average force constant (K) was calculated using following relation:

$$K = \frac{K_t + K_o}{2} \tag{6}$$

The stiffness constant (C_{11}) and (C_{12}) were calculated using the following relation [28] and the results are shown in Table-3.

$$C_{11} = \frac{K}{a} \tag{7}$$

where K is average force constant and a is lattice constant.

$$\text{Stiffness constant } (C_{12}) = \frac{\sigma C_{11}}{(1 - \sigma)} \tag{8}$$

where σ is Poisson ratio.

The Poisson ratio is function of pore fraction (σ = 0.324 × 1-1.043 f). Using eqns 7 and 8, the stiffness constant is calculated and the variation is tabulated in Table-3. It is observed from Fig. 6, both stiffness constants were decrease with increase in Cu^{2+} substitution. The values of Poisson's ratio were determined using the relation discussed elsewhere [29] and the values are presented in Table-3.
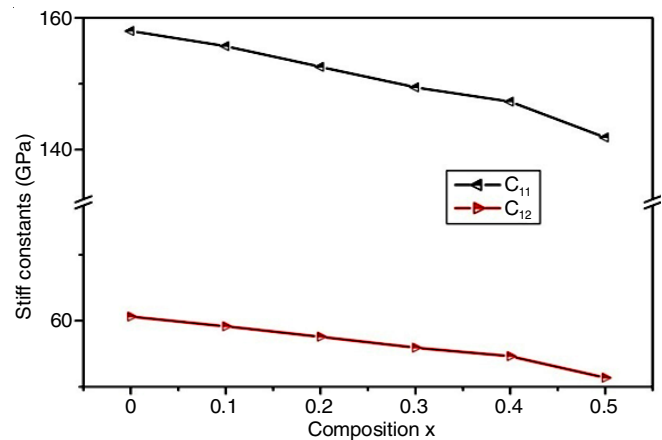
Fig. 6. Variation of stiffness constants (C_{11} and C_{12}) with Cu^{2+} content

The Poisson ratio is lies in between 0.276 and 0.266. These values are lie in the range of 1 to 0.5, which is in agreement with the theory of isotropic elasticity [30]. The other elastic moduli for cubic structure are calculated using following relation [31]:

$$\text{Rigidity modulus} (G) = \frac{E}{2(\sigma + 1)} \tag{9}$$

The rigidity modulus (G) is calculated using eqn. 9 and the variation are presented in Fig. 7. Bulk modulus (B), rigidity modulus (G), young modulus (E) decreases with increase in Cu^{2+} content, it indicates that deformation of the solid is easy and the solid has less tendency to spring back to its equilibrium position [27]. According to Wooster [32], the decrease in the modulus attributed inter-atomic bonding between Cu, Zn, Ni, Fe ions in present ferrite system.
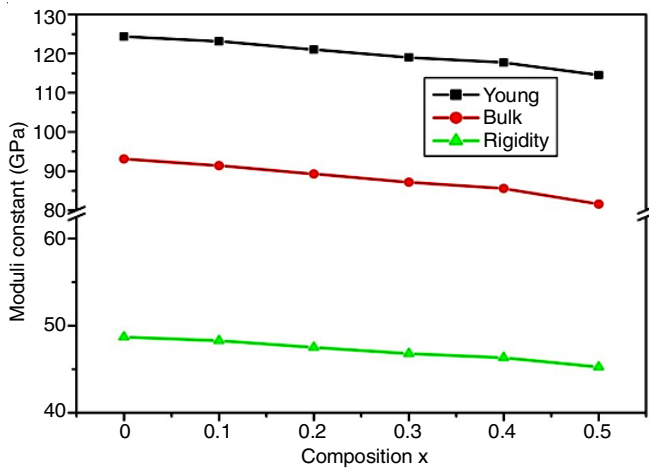
Fig. 7.   Variation of Young's modulus (E), bulk modulus (K) and modulus of rigidity (G) with Cu^{2+} content

The interatomic bonding between the various ions weaken continuously with the addition of Cu^{2+} ions therefore decreases in modulus with increasing Cu^{2+} content. The longitudinal elastic wave velocity (V_L) and transverse (shear) wave velocity (V_S) were calculated using following equations:

$$\text{Longitudinal velocity } (V_L) = \left(\frac{C_{11}}{\rho}\right)^{1/2} \qquad (10)$$

$$\text{Transverse (Shear) velocity } (V_S) = \left(\frac{G}{\rho}\right)^{1/2} \qquad (11)$$

where G is rigidity modulus with correct zero pore fraction. The values of V_L and V_S used to calculate the mean wave velocity (V_m) which is further used to calculate Debye temperature using following formula:

$$\text{Debye temperature } (\theta_E) = \frac{h}{k}\left(\frac{3\rho q N_A}{4\pi M}\right)^{1/3} \times V_m \qquad (12)$$

where h is Plank's constant, k is Boltzmann's constant, M is molecular weight, q is number if atom in the unit formula and V_m mean wave velocity.

$$\frac{3}{V_m^3} = \frac{1}{V_L^3} + \frac{2}{V_S^3} \qquad (13)$$

The values of longitudinal wave, shearing wave and mean wave velocity were calculated using eqns. 10, 11 and 13 respectively.

The longitudinal elastic wave velocity is decreases whereas transverse (shear) wave velocity increased with Cu^{2+} substitution [27]. The variation of Debye temperature (θ_E) is given Fig. 5. The Debye temperature increased with Cu^{2+} substitution. It suggested that lattice vibrations are hindered due to Cu^{2+} substitution. This may be due to the fact that strength of interatomic bonding increases with concentration (x and y) as supported by present results on the variation of elastic moduli [25].

Conclusion

The copper substituted $Ni_{0.5}Cu_xZn_{0.5-x}Fe_2O_4$ (x = 0.0, 0.1, 0.2, 0.3, 0.4 and 0.5) ferrite nanoparticles were prepared by sol-gel auto-combustion technique. All the precursors sintered at 400 °C for 4 h. The stoichiometry and single phase cubic spinel structure confirmed from EDAX and XRD patterns, respectively. The infrared spectroscopy technique was used to locate the band position of the vibration. The band frequency ν_1 and ν_2 slightly decreased to increases the Cu^{2+} ion doped contents. These variations in band frequency is due to the distributions of Cu^{2+}, Zn^{2+}, Fe^{3+} ions in A and B sites. The elastic properties such as elastic wave velocity, elastic constant and Debye temperature determined using structural and IR data. The stiffness constants (C_{11} and C_{12}) and elastic moduli decreases while Debye temperature increases with copper substitution.

CONFLICT OF INTEREST

The authors declare that there is no conflict of interests regarding the publication of this article.

REFERENCES

1.   K.A. Mohammed, A.D. Al-Rawas, A.M. Gismelseed, A. Sellai, H.M. Widatallah, A. Yousif, M.E. Elzain and M. Shongwe, *Physica B*, **407**, 795 (2012);
https://doi.org/10.1016/j.physb.2011.12.097.

2.   Y. Li, Q. Li, M. Wen, Y. Zhang, Y. Zhai, Z. Xie, F. Xu and S. Wei, *J. Electron Spectrosc. Rel. Phenom.*, **160**, 1 (2007);
https://doi.org/10.1016/j.elspec.2007.04.003.

3.   P.Y. Lee, K. Ishizaka, H. Suematsu, W. Jiang and K. Yatsui, *J. Nanopart. Res.*, **8**, 29 (2006);
https://doi.org/10.1007/s11051-005-5427-z.

4.   Y. Zhihao and Z. Lide, *Mater. Res. Bull.*, **33**, 1587 (1998);
https://doi.org/10.1016/S0025-5408(98)00164-0.

5.   G.R. Dube and V.S. Darshane, *J. Mol. Catal.*, **79**, 285 (1993);
https://doi.org/10.1016/0304-5102(93)85108-6.

6.   T.K. Kundu and S. Mishra, *Bull. Mater. Sci.*, **31**, 507 (2008);
https://doi.org/10.1007/s12034-008-0079-0.

7.   A. Pavlovitch, *J. Phys. IV FRANCE*, **7**, C1 (1997);
https://doi.org/10.1051/jp1:1997124.

8.   M.Y. Lodhi, K. Mahmood, A. Mahmood, H. Malik, M.F. Warsi, I. Shakir, M.A. Muhammad and A. Khan, *Curr. Appl. Phys.*, **14**, 716 (2014);
https://doi.org/10.1016/j.cap.2014.02.021.

9.   R.N. Panda, J.C. Shih and T.S. Chin, *J. Magn. Magn. Mater.*, **257**, 79 (2003);
https://doi.org/10.1016/S0304-8853(02)01036-3.

10.   K.B. Modi, U.N. Trivedi, P.U. Shrama, V.K. Lakhani, M.C. Chhantbar, H.H. Joshi, *Indian J. Pure Appl. Phys.*, **44**, 165 (2006).

11.   K.B. Modi, S.J. Shah, N.B. Pujara, T.K. Pathak, N.H. Vasoya and I.G. Jhala, *J. Mol. Struct.*, **1049**, 250 (2013);
https://doi.org/10.1016/j.molstruc.2013.06.051.

12.   R.D. Waldron, *Phys. Rev.*, **99**, 1727 (1955);
https://doi.org/10.1103/PhysRev.99.1727.

13.   T.T. Srinivasan, C.M. Srivastava, N. Venkataramani and M.J. Patni, *Bull. Mater. Sci.*, **6**, 1063 (1984);
https://doi.org/10.1007/BF02743958.

14.   H.M. Zaki and H.A. Dawoud, *Physica B*, **405**, 4476 (2010);
https://doi.org/10.1016/j.physb.2010.08.018.

15.   S.M. Patange, S.E. Shirsath, S.P. Jadhav, V.S. Hogade, S.R. Kamble and K.M. Jadhav, *J. Mol. Struct.*, **1038**, 40 (2013);
https://doi.org/10.1016/j.molstruc.2012.12.053.

16.   D.-H. Chen and X.-R. He, *Mater. Res. Bull.*, **36**, 1369 (2001);
https://doi.org/10.1016/S0025-5408(01)00620-1.

17.   V.V. Awati, S.M. Rathod, S.E. Shirsath and M.L. Mane, *J. Alloys Compd.*, **553**, 157 (2013);
https://doi.org/10.1016/j.jallcom.2012.11.045.

18.   S. Güner, S. Esir, A. Baykal, A. Demir and Y. Bakis, *Superlatt. Microstruct.*, **74**, 184 (2014);
https://doi.org/10.1016/j.spmi.2014.06.021.

19.   M.A. Rahman, M.A. Rahman and A.K.M.A. Hossain, *J. Magn. Magn. Mater.*, **369**, 168 (2014);
https://doi.org/10.1016/j.jmmm.2014.06.033.

20. L. Vegard, *Z. Physik*, **5**, 17 (1921);
    https://doi.org/10.1007/BF01349680.

21. B.P. Ladgaonkar, P.N. Vasambekar and A.S. Vaingankar, *J. Mater. Sci. Lett.*, **19**, 1375 (2000);
    https://doi.org/10.1023/A:1006713518433.

22. H.A. Jahn and E. Teller, *Proc. R. Soc. Lond. A Math. Phys. Sci.*, **161**, 220 (1937);
    https://doi.org/10.1098/rspa.1937.0142.

23. M C Chhantbar, U N Trivedi, P V Tanna, H J Shah, R P Vara, H H Joshi and K B Mod, *Indian J. Phys.*, **78A**, 321 (2004).

24. E.W. Gorter, *Philips Res. Rep.*, **9**, 295 (1954).

25. S.A. Mazen, T.A. Elmosalami, *ISRN Condens. Matter Phys.*, **Article ID 820726** (2011);
    https://doi.org/10.5402/2011/820726.

26. K.B. Modi, M.C. Chhantbar and H.H. Joshi, *Ceram. Int.*, **32**, 111 (2006);
    https://doi.org/10.1016/j.ceramint.2005.01.005.

27. S.E. Shirsath, S.M. Patange, R.H. Kadam, M.L. Mane and K.M. Jadhav, *J. Mol. Struct.*, **1024**, 77 (2012);
    https://doi.org/10.1016/j.molstruc.2012.05.014.

28. V.G. Patil, S.E. Shirsath, S.D. More, S.J. Shukla and K.M. Jadhav, *J. Alloys Compd.*, **488**, 199 (2009);
    https://doi.org/10.1016/j.jallcom.2009.08.078.

29. S.S. Bhatu, V.K. Lakhani, A.R. Tanna, N.H. Varsoya, J.U. Buch, P.U. Sharma, U.N. Trivedi, H.H. Joshi and K.B. Modi, *Indian J. Pure Appl. Phy.*, **45**, 596 (2007).

30. P.B. Belavi, L.R. Naik and G.N. Chavan, *J. Shivaji Univ. (Sci. Technol.)*, **41**, 2 (2014-2015).

31. V.G. Patil, S.E. Shirsath, S.D. More, S.J. Shukla and K.M. Jadhav, *J. Alloys Compd.*, **488**, 199 (2009);
    https://doi.org/10.1016/j.jallcom.2009.08.078.

32. W.A. Wooster, *Rep. Prog. Phys.*, **16**, 62 (1953);
    https://doi.org/10.1088/0034-4885/16/1/302.